university of groningen

University Medical Center Groningen

University of Groningen

Electric field modulation of spin and charge transport in two dimensional materials and complex oxide hybrids

Ruiter, Roald

IMPORTANT NOTE: You are advised to consult the publisher's version (publisher's PDF) if you wish to cite from it. Please check the document version below.

Document Version
Publisher's PDF, also known as Version of record

Publication date:
2017

Link to publication in University of Groningen/UMCG research database

Citation for published version (APA):
Ruiter, R. (2017). *Electric field modulation of spin and charge transport in two dimensional materials and complex oxide hybrids*. [Thesis fully internal (DIV), University of Groningen]. Rijksuniversiteit Groningen.

Copyright
Other than for strictly personal use, it is not permitted to download or to forward/distribute the text or part of it without the consent of the author(s) and/or copyright holder(s), unless the work is under an open content license (like Creative Commons).

The publication may also be distributed here under the terms of Article 25fa of the Dutch Copyright Act, indicated by the "Taverne" license. More information can be found on the University of Groningen website: https://www.rug.nl/library/open-access/self-archiving-pure/taverne-amendment.

Take-down policy
If you believe that this document breaches copyright please contact us providing details, and we will remove access to the work immediately and investigate your claim.

Downloaded from the University of Groningen/UMCG research database (Pure): http://www.rug.nl/research/portal. For technical reasons the number of authors shown on this cover page is limited to 10 maximum.

Download date: 04-10-2024

2

THEORETICAL CONCEPTS

ABSTRACT

This chapter will describe most of the theoretical background which is needed to understand the material in this thesis. First a general introduction will be given on spintronics and how spin currents can be generated and measured. Two different measurement geometries will be treated: the non-local and the three terminal geometry. In these geometries we use so called Hanle precession measurements to characterise the spin lifetimes. This is followed by a brief description of the conductivity mismatch problem which can have a large influence on the spin accumulation and transport. Then several different mechanisms which can cause spin relaxation will be introduced. Next, the electrostatics of metal semiconductor interfaces will be introduced and the last part introduces the materials used in this thesis: graphene, MoS_2 and (Nb:)$SrTiO_3$.

2.1 SPINTRONICS

Spintronics is the field which studies the behaviour and manipulation of spins from single or ensembles of electrons, nuclei, defects etc. In order to study the ensembles, an imbalance needs to be generated between the spin-up and spin-down electrons. This can be done in numerous ways such as by: polarised light [1], with high spin-orbit coupling materials [2, 3] or by using a ferromagnetic (FM) material [4]. In this thesis FMs are used to create spin polarized currents in non-magnetic (NM) materials. This is a commonly used method ever since the discovery of the giant magnetoresistance (GMR) effect, for which a Nobel prize was awarded to its discoverers: Albert Fert and Peter Grünberg [5, 6]. A major reason for the prize was the practical significance of the GMR effect, as the principle is still widely used in read heads of hard drives and other devices.

In the following sections I will discuss how spin currents can be generated in NM materials and which difficulties might arise during this process. Furthermore I will discuss which measurement geometries and methods that can be used to characterise the properties of electron spins in a material. Finally I will discuss several mechanisms which can cause the spins to relax.

2.2 SPIN INJECTION AND DETECTION IN NON-MAGNETIC MATERIALS

A charge current density can be viewed as the sum of both a spin-up ($\uparrow$) and spin-down ($\downarrow$) current density, or $J = J_\uparrow + J_\downarrow$. If $J_\uparrow$ and $J_\downarrow$ are not equal a spin current density is obtained of magnitude: $J_s = J_\uparrow - J_\downarrow$, where: $J_{\uparrow,\downarrow} = -\sigma_{\uparrow,\downarrow}\nabla\mu_{\uparrow,\downarrow}/q$, and $\mu_{\uparrow,\downarrow}$ is the spin-dependent chemical potential, $\sigma_{\uparrow,\downarrow}$ is the spin-dependent conductivity and q is the electron charge.

A common way to generate spin currents is by using FM materials. As shown below, inside a FM there is an unequal amount of up- and down-spins, shown by the red and blue arrows. The net magnetisation $\vec{M}$ of the FM is indicated by the arrow and is not always in the same direction as the majority of the spins involved in transport.[1] Whenever a current is sent from the FM to the NM, the imbalance of spins is transported into the NM. Because a NM is not magnetic, there can be no imbalance between the spin species in equilibrium. Therefore at a certain distance from the interface the imbalance will disappear through diffusion and relaxation of the spins. The length scale associated with this relaxation is called the spin relaxation length and functions as an important parameter in the field of spintronics.

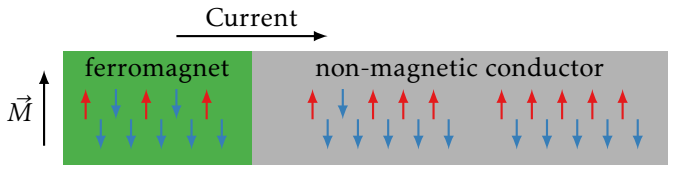

[1] The net magnetisation depends on the density of states (DOS) difference of all occupied states below Fermi level (E_F). On the other hand the spin polarisation of the current is determined by the DOS difference close to E_F.

The origin of the magnetism in FMs can be found when looking at their density of states (DOS), as shown below. At the Fermi level (E_F) the DOS for spin-up and spin-down electrons are different. This difference results in a spin dependent conductivity, which for a diffusive system is given by the (spin dependent) Einstein relation:

$$\sigma_{\uparrow,\downarrow} = D(E)_{\uparrow,\downarrow} q^2 \nu(E)_{\uparrow,\downarrow},$$

where the indices $\uparrow,\downarrow$ denote a up-spin or down-spin, D is the diffusion constant, E is the energy, q the electron charge and ν is the DOS. As we saw earlier, this leads to different current densities for spin-up and spin down via $J_{\uparrow,\downarrow} = -\sigma_{\uparrow,\downarrow} \nabla \mu_{\uparrow,\downarrow}/q$.

When a current is sent from the FM into a NM material, the spin imbalance will be projected onto the DOS of the NM, which has a symmetric DOS. This gives rise to a spin chemical potential difference, which is defined as: $\mu_s = (\mu_\downarrow - \mu_\uparrow)/2$. Furthermore we also define an average chemical potential: $\mu_o = (\mu_\downarrow + \mu_\uparrow)/2$, which is equal to the E_F for metals and degenerate semiconductors [7, p. 26]. Since in equilibrium $\mu_s = 0$, as shown on the right, μ_s will decay as it moves further away from the FM/NM interface.

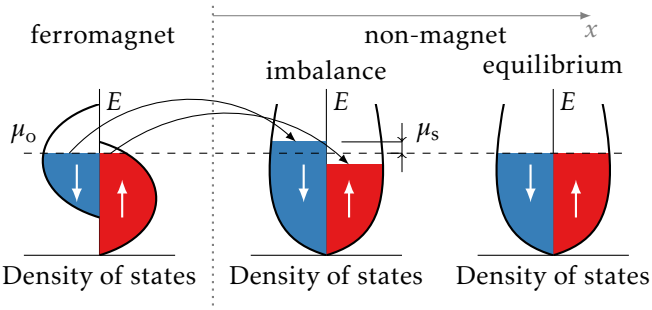

The decay of the spin chemical potential in the NM can be modelled by looking at the Bloch equation in a steady-state [7, p. 24]:

$$\frac{d\vec{\mu}_s}{dt} = D_s \nabla^2 \vec{\mu}_s - \frac{\vec{\mu}_s}{\tau_s} = 0,$$

where $\vec{\mu}_s = (\mu_x, \mu_y, \mu_z)$ is the spin accumulation in three dimensions, D_s is the spin diffusion constant and τ_s is the spin relaxation time. We can solve this equation for one dimensional transport, for example in the x-direction. In an infinite 1D channel, the boundary conditions are: $\mu_s(x = \infty) = 0$ and $\mu_s(x = 0) = \mu_{s,o}$; where $\mu_{s,o}$ is the chemical potential at the FM/NM interface. This then leads to a general solution: $\mu_s = \mu_{s,o} e^{-x/\lambda_s}$, where $\lambda_s = \sqrt{D_s \tau_s}$ and is called the spin relaxation length. Thus the spin signal decays exponentially with distance away from the FM/NM interface, inside the NM.

2.3 LOCAL SPIN VALVES

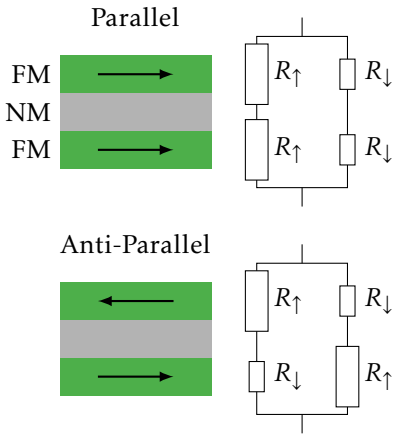

In order to detect a spin accumulation and characterise the spin properties of a NM material, another FM is placed at the other end of the NM material, as shown on the right. These are referred to as local spin-valves. The arrows denote the net magnetisation of the FM. To describe the resistance of such a spin valve, often a so called two-channel model is used [8, 9]. In this model the spin channels are represented by resistances $R_{\uparrow,\downarrow}$, as shown in the figure on the right. Here we neglect the resistance of the NM, as it is not spin dependent. It follows from $\sigma_{\uparrow,\downarrow} = D(E)_{\uparrow,\downarrow} q^2 \nu(E)_{\uparrow,\downarrow}$ and the fact that $\nu_\uparrow \neq \nu_\downarrow$ for a FM, that the resistances are different for the $\uparrow$ and $\downarrow$ channels. In this example, when both FMs are parallel, spin-up (spin-down) electrons experience a high (low) resistance in both FM layers. On the other hand in the case of anti-parallel aligned FMs, both spin species experience once a high resistance and once a low resistance. Thus in the case of parallel aligned electrodes a lower resistance is expected than for the anti-parallel one.

2.4 NON-LOCAL SPIN VALVES

A non-local geometry can be used to probe spin currents, as shown in the figure. In this geometry the current path is separated from the voltage detection contacts. The contacts in the figure are denoted as numbered red blocks and depict FM contacts which have a certain magnetisation along the x-direction, as shown in the top view. The grey bar depicts the channel through which the electrons and spins can travel.

Spin polarised electrons are injected into the channel below the second ferromagnetic electrode (FM2) and diffuse in all directions, as indicated by the black gradient. The spins in the channel can be detected by the two voltage contacts FM3 and FM4. As there is no net current between electrodes FM2 and FM3, but only a spin current, this geometry should prevent spurious charge induced effects [7]. However, in practise there can be (magnetic field dependent) background signals due to Peltier/Seebeck effects or non-ideal contacts [10–12].

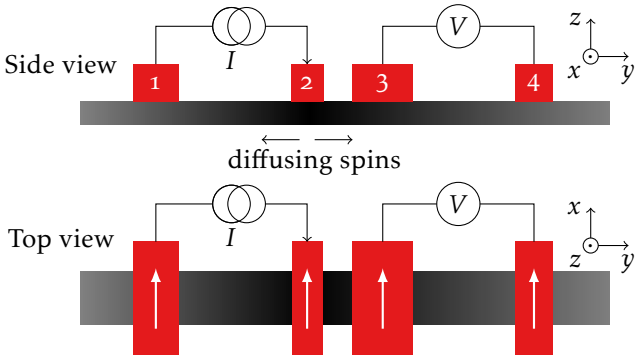

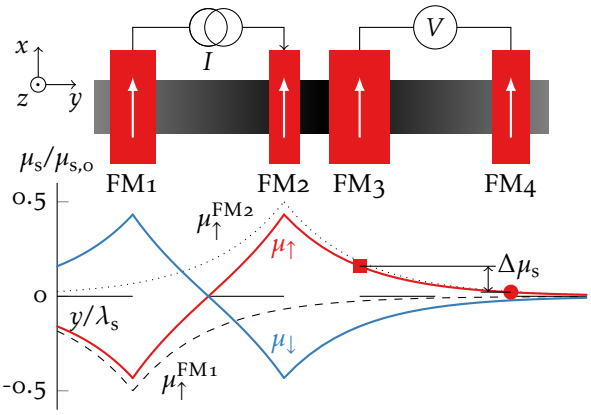

A better understanding of the spin signals can be obtained by looking at the spin dependent chemical potential μ_s, as shown on the vertical axis in the graph on the right. The potential μ_s is normalised by the spin chemical potential at the injection point $\mu_{s,o}$. The horizontal axis denotes the length of the channel y, normalised by the spin relaxation length λ_s. The length of a single dash $y/\lambda_s = 1$. Above the graph, the measurement circuit is drawn, where the arrows denote the magnetisation direction of the different electrodes.

If a current is injected through the second FM contact, FM2, it generates a spin chemical potential potential indicated by the dotted lines in the graph as $\mu_\uparrow^{FM2}$ and the black gradient around FM2 in the channel. The decay of the signal is due to the aforementioned diffusion and relaxation of the spins. The amplitude of 0.5 below the contacts is because electrons can diffuse into two directions, see section 2.4.1. At FM1, spin-up electrons are extracted from the channel and this gives rise to a negative $\mu_\uparrow^{FM1}$. By adding $\mu_\uparrow^{FM2}$ and $\mu_\uparrow^{FM1}$ we obtain $\mu_\uparrow$ as indicated by the red line. A similar approach also gives $\mu_\downarrow$, indicated by the blue line. Finally the spin signal is probed by FM3 and FM4, indicated by —■— and —●— respectively. In this case both electrodes probe the potential of $\mu_\uparrow$ and the size of the spin signal is proportional to $\Delta\mu_s$.

A magnetic field can be applied in the $-x$-direction in order to switch some of the contacts into a different orientation. This is because the width of a contact determines the field which is required to reverse its magnetisation. The narrower a contact, the higher the field is needed to reverse its magnetisation. Since FM1 and FM3 are the widest, they will switch first.

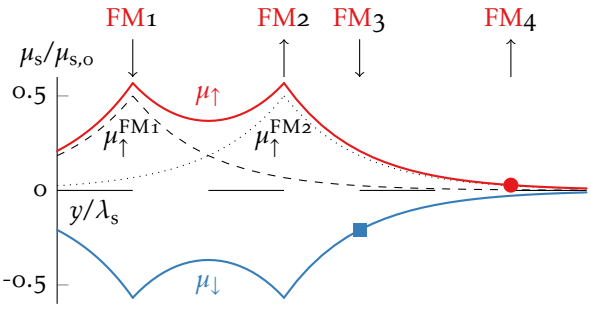

After switching both contacts, a potential profile as shown on the right is obtained. Here, FM2 still injects spin-up electrons, but FM1 now *extracts* spin-down electrons. This is effectively the same as an injection of spin-up electrons. Thus also at FM1, a spin-up accumulation is created and the potential of $\mu_\uparrow = \mu_\uparrow^{FM1} + \mu_\uparrow^{FM2}$ is increased. Finally FM3 now senses the spin-down channel, as indicated by —■—, and the measured $\Delta\mu_s$ will have an opposite sign, as compared to the previous configuration where all the electrodes were parallel.

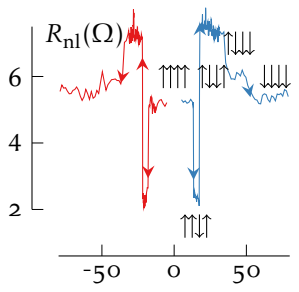

A typical measurement of a non-local spin valve is shown here on the right. For such a measurement, the measured voltage is also referred to as the non-local voltage V_{nl} and from this we can calculate the non-local resistance $R_{nl} = V_{nl}/I$. The non-local voltage is measured, while sweeping an in-plane magnetic field B. First, all the electrodes are aligned into one direction, by applying a large in-plane magnetic field. Then the magnetic field turned off and slowly ramped into the opposite direction (indicated by the red and blue arrows), reversing the magnetisation of the electrodes one-by-one (indicated by the vertical arrows). At each reversal, a stepwise increase or decrease in the non-local resistance is seen.

Note that this signal also has a significant background signal, due to the aforementioned Peltier/Seebeck effects or non-ideal contacts [10–12]. Four switches can be observed, because all contacts are within a few times the spin relaxation length. However, it is usually preferred to only see a two switches ( ), as this mitigates the analyses of the spin signals. Preventing additional switches can be done by placing the outer contacts at least a few λ_s away from the inner contacts, although this is not always possible for practical reasons.

2.4.1 *Non-local spin signals in a two-dimensional channel*

Here I will briefly discuss how the size of the non-local resistance can be calculated. Again we use the spin diffusion equation in the steady-state condition [7, p. 24]:

$$\frac{\mathrm{d}\vec{\mu}_s}{\mathrm{d}t} = D_s \nabla^2 \vec{\mu}_s - \frac{\vec{\mu}_s}{\tau_s} = 0,$$

where $\vec{\mu}_s = (\mu_x, \mu_y, \mu_z)$ is the spin accumulation in three dimensions, D_s is the spin diffusion constant and τ_s is the spin relaxation time. Since for a 2D channel there is no thickness and the spin accumulation is assumed to be constant across the width of the flake, only the spin accumulation in one direction is considered.

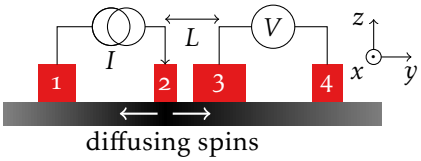

The boundary conditions for this case are slightly different than the ones from section 2.2. This is because the spins can diffuse into two directions, as shown by the black gradients moving away from contact 2 in the figure on the right. The boundary conditions become: $\mu_s(y = \pm\infty) = 0$. This then leads to a general solution: $\mu_s = \mu_{s,o}/2e^{-|y|/\lambda_s}$, where $\lambda_s = \sqrt{D_s \tau_s}$ and $\mu_{s,o}$ is the chemical potential below the injection contact and the factor two comes from the fact that the electrons diffuse into two directions. The size of $\mu_{s,o}$ is given by:

$$\mu_{s,o} = qP_i I R_{sq} \lambda_s / W,$$

where q is the electron charge, P_i is the polarisation of the injection electrode, I is the current, R_{sq} is the square resistance and W is the width of the channel.

The spin chemical potential is then sensed by the two detection contacts: one at a distance L from the injection contact and the other at infinity. This results in a non-local voltage:

$$V_{nl} = P_d/q\,(\mu_s(L) - \mu_s(\infty)),$$

where P_d is the polarisation of the detector electrode. Using $\mu_s(\infty) = 0$ we obtain for the non-local resistance:

$$R_{nl} = \frac{P_i P_d R_{sq} \lambda_s}{2W} e^{-L/\lambda_s}.$$

For simplicity it is usually assumed that $P_i = P_d$.

2.5 THREE TERMINAL MEASUREMENTS

Another possible measurement geometry is the three terminal measurement geometry. This geometry can be seen as a non-local geometry, where the two inner contacts are merged, as shown below. The outer contacts are usually placed at distances many times the spin relaxation length and thus probe the equilibrium state in the channel ($\mu_s = 0$). This measurement geometry can be advantageous when the spin relaxation length is very short and thus spins can not reach a detector electrode, within practical injector-detector distances in a non-local geometry. However, there are also some drawbacks. Because in a three terminal geometry the same contact is used for injection *and* detection of electron spins, the measured voltage drop consists of both a charge and spin related part. This makes the three terminal (3T) geometry more prone to all kinds of spurious magnetoresistance (MR) effects, which are sometimes hard to discern from a normal Hanle spin precession measurement. See chapter 2.6 for an explanation of the Hanle effect and see reference [13, chapter 1.3] for the standing issues related to three terminal spin injection.

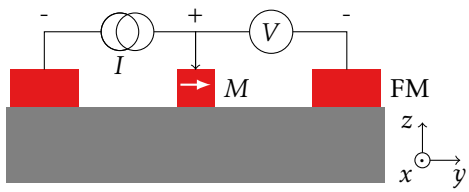

2.5.1 *Three terminal spin signals in a three dimensional channel*

The fact that the three terminal geometry uses one electrode for both injection and detection, results in an chemical potential beneath the FM contact, consisting of a charge and spin related part: $\mu_{3T} = \mu_o + \mu_s$. The charge contribution comes from: $\mu_o = (\mu_\downarrow + \mu_\uparrow)/2$ and the spin contribution from:

$$\mu_s = (\mu_\downarrow - \mu_\uparrow)/2 = qP_i I \rho \lambda_s / A,$$

where P_i is the polarisation of the 'injector' contact, I is the current, ρ is the resistivity of the channel, λ_s is the spin relaxation length in the channel and A is the area of the contact.

Since there is no charge current at the outer voltage contact nor a spin accumulation, this means that the measured voltage drop is entirely determined by the central contact. We then have:

$$V_{3T} = V_o + P_d \mu_s / q = V_o + P_d P_i I \rho \lambda_s / A,$$

where V_o is the charge voltage drop which is determined by the resistance of the FM/NM interface and the resistance of the channel below the contact and P_d is

the detector polarisation. Because this is the same contact as the injection one we obtain:

$$V_{3T} = V_0 + P^2 I \rho \lambda_s / A.$$

2.6 HANLE SPIN PRECESSION

When the center of mass of a spinning top (with angular momentum $\vec{L}$) is not directly above the contact point with the ground, gravity $\vec{F}_g$ can exert a torque $\vec{T}$ on the top. As a consequence the top will start precessing as shown on the picture on the right [14, p. 37].

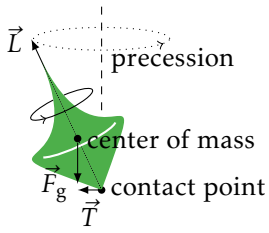

Similarly when an electron spin is subjected to a perpendicular magnetic field $B_\perp$ it will start precessing. Here the magnetic field and the spin angular momentum are analogous to the gravitational force and angular momentum $\vec{L}$ from the spinning top example. The precession frequency of the electron spin is known as the Lamor frequency and is given by:

$$\omega_L = -\frac{g\mu_B B_\perp}{\hbar},$$

where $g \approx 2$ is the g-factor, μ_B is the Bohr magneton and $\hbar$ is the reduced Planck constant.

2.6.1 *Non-local geometry*

The figure on the right shows Hanle spin precession in a non-local geometry. Spins are injected on the left and diffuse to the right where they are detected. When a perpendicular magnetic field (B_z in the figure) is applied, the spins start to precess. The rotation angle of the electrons at the voltage probe depends on the size of the magnetic field and the travel time of the electrons. The projection of the electron spin on the magnetisation axis of the voltage contact determines the size of V. For clarity this picture shows the case of a ballistic electron e^- ●——→ travelling the shortest route between the two contacts. In reality we measure in the diffusive regime

, thus electrons perform a random walk and V will be a macroscopic average over all electrons which travelled to the voltage probe via different paths.

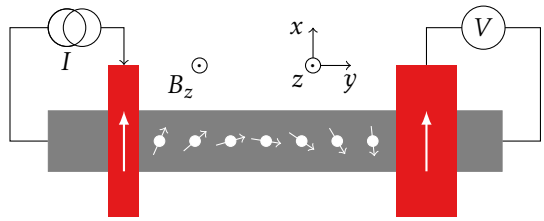

A plot of the measured non-local resistance versus the out-of-plane magnetic field B is shown on the right. At $B = 0$ the electron spin will not precess, thus R_{nl} is maximum. Upon increasing the magnetic field, the non-local resistance decreases and becomes zero when the average projection of the spins is perpendicular to the magnetisation of the voltage probe. At slightly higher field values the spins have rotated 180° and $R_{nl} < 0$, but

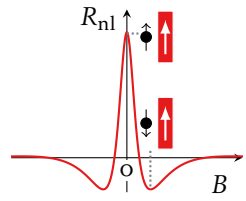

the size of R_{nl} here is smaller than at $B = 0$. The reduced R_{nl} is due to the different travelling times of the individual electrons, which increases the spread in precession angles of the detected spins. If the magnetic field is increased even more, R_{nl} is reduced again.

The observed behaviour of R_{nl} versus B can be modelled in the diffusive regime by looking at the probability distribution of an electron which diffuses a distance L from an injection towards a detection electrode as a function of time [15]:

$$\mathcal{P}_D(t) = (4\pi D_s t)^{-1/2}\, e^{-L^2/(4D_s t)}.$$

We can include spin relaxation by multiplying the above with e^{-t/τ_s} and we multiply with $\cos(\omega_L t)$ to include spin precession:

$$\mathcal{P}(t) = (4\pi D_s t)^{-1/2}\, e^{-L^2/(4D_s t)} e^{-t/\tau_s} \cos(\omega_L t).$$

Integration of the above over time yields the spin accumulation:

$$\mu_s(L,B) = 2\mu_{s,0}\sqrt{\frac{D_s}{\tau_s}}\int_0^\infty \mathcal{P}(t)\mathrm{d}t,$$

where the pre-factor $2\sqrt{D_s/\tau_s}$ comes from the boundary condition $\mu_s(L = 0, B = 0) = \mu_{s,0}$.

This integral can be solved with the help of a mathematical software, such as Wolfram Mathematica. Finally we use $R_{nl} = \mu_s P_d/(eI)$ to obtain:

$$R_{nl}(L,B) = \pm\frac{P_i P_d R_{sq} D_s}{W}\,\Re\mathfrak{e}\left(\frac{1}{2\sqrt{D_s}}\,\frac{e^{-L\sqrt{\lambda_s^{-1} - i\omega_L/D_s}}}{\sqrt{\tau_s^{-1} - i\omega_L}}\right).$$

Using this expression D_s and τ_s (and P if R_{sq} is known) can be extracted from Hanle measurements.

2.6.2 *Three terminal geometry*

In a three terminal (3T) geometry spins are injected *and* detected by the same contact, therefore the intuitive picture sketched for Hanle measurements in a non-local geometry is not valid. Instead, a 3T Hanle measurement can be visualised as shown on the right. Here a FM is shown which injects a spin into a NM at $t = t_0$. An out-of-plane magnetic field B dephases the injected spin. At $t = t_1$ the next spin is injected into the NM, while the t_0 spin has rotated by a certain angle. Again a short while later at $t = t_2$ an additional spin is injected and the previously injected spins have both rotated. This dephasing goes faster as the magnetic field is increased, thus the spin accumulation underneath the FM decreases at higher field values.

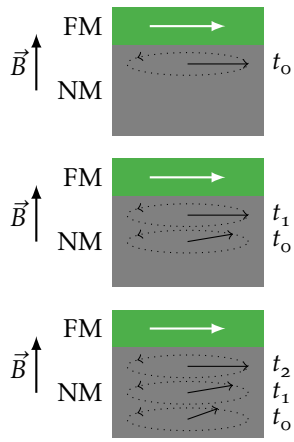

The dimensions of the inner contact are much larger than the spin relaxation length λ_s and therefore the spin accumulation is constant underneath the entire contact. Additionally, because all the dephasing occurs underneath the contact, drift and diffusion are not expected to influence the Hanle profile.

This can be viewed as a 0D system in steady-state, which is described by the Bloch equation, without drift or diffusion [16]: $\vec{\mu}_s(x,y)/\tau_s = \vec{\omega}_L \times \vec{\mu}_s(x,y)$. The solution gives a Lorentzian:

$$\mu_s(B) = \frac{\mu_s(B=0)}{1+(\omega_L \tau_s)^2}.$$

However, there can still be diffusion away from the FM/NM interface. Including this will lead to the following [17, supplementary]:

$$\mu_s(B) = \frac{\mu_s(B=0)}{\sqrt{2}} \sqrt{\frac{1+\sqrt{1+(\omega_L \tau_s)^2}}{1+(\omega_L \tau_s)^2}}.$$

2.7 CONDUCTIVITY MISMATCH PROBLEM

So far we have been neglecting an important aspect of spin injection from a well conducting FM into a relatively poor conducting NM channel. Because of the large mismatch in conductivity, spins can easily flow back into the FM contact where they rapidly lose their initial spin, due to the short spin lifetime inside the FM. This problem was first discussed by Schmidt *et al.* [18] and is known as the conductivity mismatch problem.

It turns out that the polarisation of the current injected into the NM P_J is not simply the polarisation of the FM P_{FM}, but is given by [19]:

$$P_J = \frac{P_{FM}}{1+R_{NM}/R_{FM}},$$

where the spin resistance of the FM and NM are given by $R_{NM,\,FM} = \lambda_s^{NM,\,FM}/\sigma_{NM,\,FM}$, where λ_s is the spin relaxation length and σ is the conductivity. From this it is clear that $P_J = P_{FM}$ only if $R_{NM} \ll R_{FM}$.

In order to circumvent the problem of a reduced P_J in cases where $R_{NM} > R_{FM}$, a highly resistive barrier can be inserted between the FM and NM, thereby changing the above formula into [19]:

$$P_J = \frac{P_{FM}R_{FM} + P_B R_B}{R_{FM}+R_{NM}+R_B},$$

where R_B and P_B are the resistance and polarisation of the barrier respectively.

Now, if we have $R_{FM} \ll R_{NM}$ and $R_{FM} \ll R_B$, P_J becomes:

$$P_J = \frac{P_B R_B/R_{NM}}{R_B/R_{NM}+1}.$$

Plotting P_J/P_B versus R_B/R_{NM} shows that if R_B is smaller than R_{NM}, the polarisation of the current P_J is severely reduced. Once $R_B \gtrsim 10 R_{NM}$, P_J is not affected anymore and the conductivity mismatch has been circumvented.

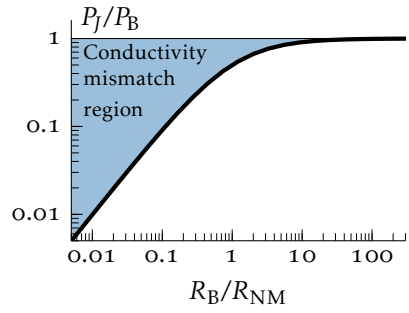

2.8 SPIN RELAXATION

Until now we have seen that the electron spin gets randomised on a typical time scale, referred to as the spin relaxation time τ_s. But we have not discussed the mechanisms which can cause this relaxation.

In order to explain this, imagine an ensemble of spins with a total spin $\vec{s}$ and we apply a magnetic field B_0 in the z-direction. The equilibrium spin accumulation in this field is given by s_{0z} and is zero in absence of B_0. Additionally there is a oscillating field $\vec{B}_1(t)$, so that the total field is given by $\vec{B} = B_0\hat{z} + \vec{B}_1(t)$. The time evolution of the spin ensemble is then given by [7, p. 705]:

$$\frac{\partial s_x}{\partial t} = \gamma(\vec{s}\times\vec{B})_x - \frac{s_x}{T_2}, \quad \frac{\partial s_y}{\partial t} = \gamma(\vec{s}\times\vec{B})_y - \frac{s_y}{T_2} \quad \text{and} \quad \frac{\partial s_z}{\partial t} = \gamma(\vec{s}\times\vec{B})_z - \frac{s_z - s_{0z}}{T_1}.$$

Here $\gamma = g\mu_B/\hbar$ is the gyromagnetic ratio, with g the effective electron g-factor and μ_B the Bohr magneton. The time T_1 is the spin relaxation time and describes the relaxation of a non equilibrium spin population to its equilibrium value. T_2 is the spin dephasing time and describes the dephasing of spin components transverse to the magnetic field direction (in this case x and y)[2]. In experiments we often measure the time T_2 and in case of weak magnetic fields it is often the case that $T_1 = T_2 = \tau_s$, where τ_s is referred to as the spin relaxation time [7, p. 705].

Since spin dephasing and relaxation requires the presence of a magnetic field, we have to find its sources. Besides externally applied magnetic fields, electrons can also 'see' magnetic fields from their frame of reference, due to their momentum. The coupling of the electron's momentum to its spin is referred to as spin-orbit coupling (SOC).

A simple example of SOC is the case of an hydrogen atom, where from the proton's frame a negatively charged electron orbits it. But from the electron's frame it is the other way around: it sees the proton moving. Due to this moving charge, the electron sees a magnetic field $\vec{B}$. The magnetic moment $\vec{\mu}$ of the electron will start precessing around this field, just as we saw earlier with Hanle precession in section 2.6.

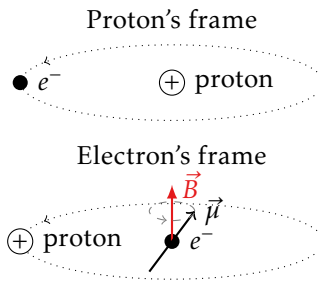

Here I will discuss two spin relaxation mechanisms where the strength of the SOC depends on the electron's momentum relaxation time τ_p, namely the Elliott-Yaffet (EY) mechanism [20, 21] and the D'yakonov-Perel' (DP) mechanism [22]. Additionally I will also treat electric fields induced SOC.

[2] T_1 is also sometimes referred to as $\tau_\perp$ and T_2 as $\tau_\parallel$.

2.8.1 *Elliot-Yafet mechanism*

The Elliott-Yaffet (EY) mechanism can be present in systems with and without an inversion centre [23, p. 309] and the relaxation depends on spin-flip scattering events. Each time the electron scatters (with an impurity, boundary, phonon etc.), there is a finite chance of a spin-flip. The odds of a spin-flip are proportional to the SOC strength. The relation between the spin relaxation τ_s and momentum scattering time τ_p is given by [23, p. 309]:

$$\frac{1}{\tau_s} = \omega_{SO}^2 \frac{\lambda_F^2}{v_F^2 \tau_p} \approx \left(\frac{E_{SO}}{E_F}\right)^2 \frac{1}{\tau_p},$$

where $E_{SO} = \hbar\omega_{SO}$ and $E_F = \hbar k_F v_F/2$ is the Fermi energy and k_F, v_F and λ_F are the wave number, velocity and wavelength of an electron at the Fermi level and ω_{SO} is the SOC induced precession frequency.

2.8.2 *D'yakonov-Perel' mechanism*

The D'yakonov-Perel' (DP) mechanism is only present in systems without spatial inversion symmetry, such as GaAs [23, p. 309]. As opposed to EY, in the DP picture, electrons lose their information *in between* scattering events. This is due to the fact that in these systems the SOC manifests as an effective magnetic field, causing spin precession in between scattering events. Since the SOC is momentum dependent, electrons precess with a given frequency (or dephase) until they scatter into a different momentum state. The net effect of this momentum scattering is the randomisation of the precession frequencies (an effect known as motional narrowing [7, p. 715]). Therefore the τ_s and τ_p are inversely proportional for the DP mechanism [23, p. 309]:

$$\frac{1}{\tau_s} = \omega_{SO}\tau_p.$$

Thus more scattering leads to higher spin lifetimes for the DP mechanism.

2.8.3 *Electric field induced spin-orbit coupling*

The SOC induced by internal or external electric fields is usually referred to as Bychkov-Rashba (BR) SOC [7, 24, 25]. BR SOC is only present in materials which: lack inversion symmetry, where it is is broken by an electric field (such as Schottky barriers of section 2.9) or at interfaces and surfaces. It is a much broader concept and actually is the origin of spin precession in the diffusive regime of the DP mechanism [26, p. 873]. The concept is thus the same: an electric field is perceived as a magnetic field by the moving electron. This magnetic field is also referred to as the Rashba field B_R and the magnitude is given by [26, p. 873]:

$$B_R = 2\alpha_R(\mathcal{E})\frac{k_F}{g\mu_B},$$

where α_R is the Rashba parameter, k_F is the wave number at the Fermi level, $g \approx 2$ is the g-factor and μ_B is the Bohr magneton. The Rashba parameter can be tuned by the electric field strenght $\mathcal{E}$, thus thereby modulating the spin relaxation.

2.9 SCHOTTKY BARRIERS

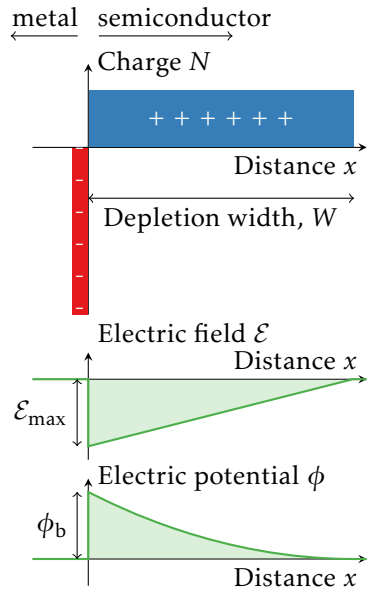

When a metal is brought into direct contact with a semiconductor and their Fermi levels are not equal, charges will flow from one to the other in order to equalise the Fermi levels. On the right we see a situation where a metal was placed on a electron doped (n-doped) semiconductor and the semiconductor's Fermi level was above that of the metal. Consequently, electrons were transferred to the metal side, leaving behind positively charged ions of the semiconductor. Because these ions are fixed and their density is quite low ($\sim 10^{19}\,\mathrm{cm}^{-3}$), ions are present at a relatively large distance from the interface, called the depletion width W. At the metal side, negative charges will screen the positive charges of the semiconductor. They will actually accumulate in a much thinner region than shown and the areas of the negative and positive charges should be the same to be charge neutral.

Between the opposing charges an electric field is generated. The field distribution inside the semiconductor can be found by using Poisson's equation: $\nabla^2\phi(x) = -qN_D/\epsilon_s$, where $\phi(x)$ is the electrostatic potential, q the electron charge, N_D the donor density and ϵ_s is the dielectric permittivity of the semiconductor. The electric field $\mathcal{E}$ can be found by integrating both sides and using the boundary conditions $\mathcal{E}(W) = 0$ and $\mathcal{E}(0) = \mathcal{E}_{max}$:

$$\nabla\phi(x) = \mathcal{E}(x) = qN_D(W - x)/\epsilon_s = \mathcal{E}_{max} - qN_D x/\epsilon_s.$$

Integrating a second time gives the electrostatic potential:

$$\phi(x) = \phi_b - qxN_D\frac{W - x}{2\epsilon_s},$$

where ϕ_b is the Schottky barrier height.

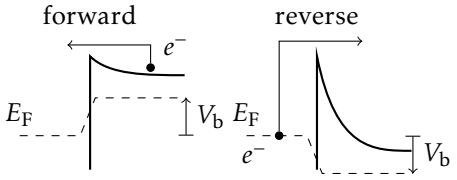

A bias voltage V_b can be applied between the metal and semiconductor, such that electrons are pushed from the semiconductor to the metal. This pushes the semiconductor bands up, relative to E_F at the metal side. Consequently, the barrier height is reduced for electrons and a current can flow in this direction. This is also referred to as the forward bias regime. On the other hand in the reverse bias regime, electrons will be pushed from the metal to the semiconducting side. The bias does not decease the barrier height seen by the electrons on the metal side, because the majority of the voltage drop will happen across the highest resistance in the circuit. Which in this case is the barrier region. Only electrons which happen to have a very high thermal energy can surpass the barrier, thus severely limiting the current in the reverse direction.

2.10 GRAPHENE

Graphite consists of layers of graphene, held together by weak van-der Waals forces at an inter layer spacing of 0.335 nm. The graphene layers are build up of carbon atoms which are arranged in a hexagonal lattice. The lattice can be build from a unit cell, spanned by the vectors:

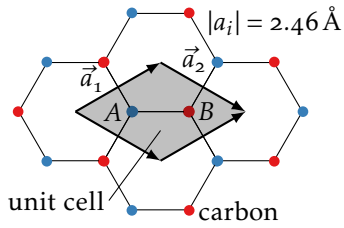

$$\vec{a}_1 = a/2\,\langle 3, \sqrt{3}\rangle \quad \text{and} \quad \vec{a}_2 = a/2\,\langle 3, -\sqrt{3}\rangle,$$

where $a = 1.42$ Å is the carbon-carbon distance. The unit cell contains two atoms labelled A and B, which are not equivalent. As a result there is a so called valley degeneracy equal to 2, next to the spin degeneracy of 2.

Ever since the first isolation of graphene in 2004 [27], it has attracted a lot of attention, due to its remarkable charge and spin transport properties. The charge transport properties of graphene are due to the special band structure of graphene. At energy values close to the Fermi level, graphene has a linear dispersion. This means that the energy E depends linearly on the wave vector k and is given by: $E \approx \pm\hbar v_F|\vec{k}|$, where $\hbar$ is the reduced Planck constant, $v_F \approx 10^6$ m/s is the Fermi velocity and $\hbar\vec{k} = \vec{p}$ is the momentum for a wave like particle [28]. This is vastly different from the usual case where the velocity changes considerably with energy, because $E = p^2/(2m_e)$, where m_e is the electron mass and $v = p/m_e = \sqrt{2E/m_e}$.

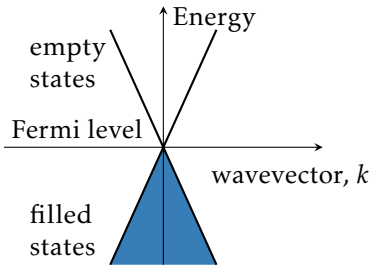

The dispersion relation of graphene actually resembles the energy of relativistic particles, which are described by the massless Dirac equation and travel at the speed of light–only in graphene the charges are moving at v_F, which is about 300 times lower than the speed of light. Due to this analogy, electrons in graphene are referred to as Dirac fermions and the cone in the $E - \vec{k}$ diagram is called a Dirac cone.

The origin of graphene's favourable spin transport properties is twofold: Firstly carbon has a low atomic mass Z, thus spin-orbit strength should be low since it increases with Z^2 [7, p. 152]. Secondly graphene consists of ~ 99 % ^{12}C [29, p. 1995], which has no nuclear spin. Based on these arguments, spin relaxation times of 1 µs were expected [30, p. 803]. However, the first experimentally obtained values were around 100-200 ps at room temperature [31]. Although the exact reason for the large discrepancy is unknown, a lot of factors seem to influence the measured spin lifetimes such as the: substrate [32], contacts [33] and graphene cleanliness [34]. Nevertheless, graphene has a longer spin relaxation length than metals and semiconductors at room temperature [30, table 2].

2.11 MOLYBDENUM DISULFIDE

In the wake of graphene's success, many more 2D materials were 'discovered'. Many were already known for years, but had not been investigated as single layered materials. A special class within the 2D materials are the transition metal dichalcogenides (TMDs). Their general formula is MX_2, where M is a transition metal atom (such as: Mo, W, etc.) and X is a chalcogen (S, Se, Te, etc.).

One of these TMDs is MoS_2 and is a semiconductor, whose properties depend on the amount of layers which are used. Single layer MoS_2 has a direct bandgap of 1.89 eV, but from two layers onwards it becomes an indirect semiconductor and its bandgap goes towards 1.29 eV for bulk MoS_2 [35]. This is also shown below, where the data has been taken from K. F. Mak *et al.* and redrawn.

Analogous to other 2D materials, bulk MoS_2 is build up from individual layers of a few atoms thick and are bound by van der Waals forces. In contrast to graphene's purely two dimensional structure, the S atoms of MoS_2 stick out of the plane defined by the Mo atoms. From the top it can be seen that the atoms are arranged in a hexagon lattice, where one Mo and two S atoms make up the unit cell (the second S atom sits below the first).

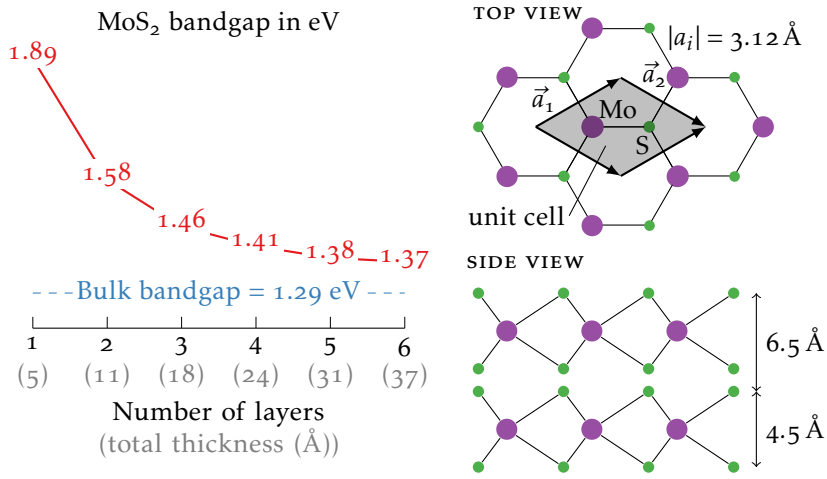

2.12 STRONTIUM TITANATE

$SrTiO_3$ (STO) is a well known insulator with an indirect bandgap of 3.25 eV and a direct bandgap of 3.75 eV in the complex oxides material class [36]. The unit cell of STO is shown on the right, where Sr ions are found at the corners, a Ti ion sits at the centre which is surrounded by an octahedron of oxygen ions. This arrangement is also called a perovskite crystal structure.

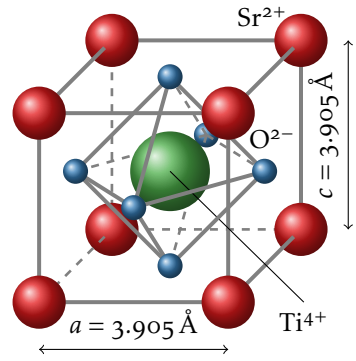

In equilibrium all the ions in STO compensate each others ionic charges. However if, for example the oxygen ion is displaced slightly from its central position, the unit cell will have a net directional polarisation $\vec{P}$. The disturbance of the equilibrium can be done by application of stress, defects or an electric field $\vec{E}$.

At room temperature STO is a linear dielectric, where upon the application of an electric field the material polarises according to $\vec{P} = \epsilon_0 \chi \vec{E}$, where ϵ_0 is the permittivity of vacuum and χ is the dielectric susceptibility. This behaviour is also referred to as paraelectricity, analogous to paramagnetism. In case of STO the $\chi \approx 300$ is quite high (compared to for example SiO_2 where $\chi = 2.9$) and it varies slightly from

sample to sample in STO.

When STO is cooled down to a few Kelvin its dielectric susceptibility increases towards 2×10^4, where a rapid increase sets in below 100 K as shown in a redrawn figure from reference [37]. Although there is some spread in χ from sample to sample, usually it reaches $\chi > 10^4$ at 4 K.

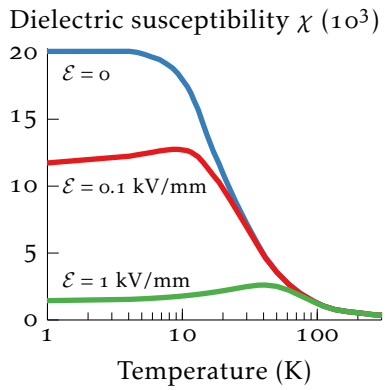

The reason for this large increase is that as STO cools down, it comes closer to a transition temperature or Curie temperature T_C. In this regime the dielectric susceptibility of a material is described by the Curie-Weiss law: $\chi = C/(T - T_C)$, where C is a material constant and T the temperature. Since the Curie-Weiss law diverges at $T \approx T_C$, it can only be used at $T > T_C$. In reference [37] they find $T_C = 35.5$ K, when fitted in a range $150 < T < 300$.

At $T < T_C$ the material wants to go into a ferroelectric phase and thus obtain a spontaneous polarisation. However, despite the fact that a double well potential develops in the vertical direction, STO does not become ferroelectric. This is because the O atoms are light enough to tunnel through the energy barrier [38, p. 120] and STO is therefore also referred to as a quantum paraelectric [37].

Another property of the dielectric susceptibility is its high sensitivity to electric fields $\mathcal{E}$. This can be modelled using [39]:

$$\epsilon_r = \frac{b(T)}{\sqrt{(b(T)/\epsilon_r)^2 + \mathcal{E}^2}} \quad \text{and} \quad b(T) = 1.37 \times 10^7 + 4.29 \times 10^5 T,$$

where $\epsilon_r = \chi + 1$ and the units of $\mathcal{E}$ are in V/cm. The results are shown in the graph above. Note that the effect is quite large, especially at low temperatures.

2.12.1 *Semiconducting strontium titanate*

STO is an insulator, but can become semiconducting when oxygen vacancies are introduced or when n-doped with Nb at the Ti sites. Nb doped STO, or Nb:STO, inherits some properties from its parent compound, such as a electric field and temperature dependent dielectric permittivity. On the other hand, it is a semiconductor whose properties behave differently then most other semiconductors. For example, there is no carrier freeze out in Nb:STO, but conductivity actually goes up with decreasing temperature [40]. This is due to a decrease of the donor bound energy $E_D \propto \epsilon_r^{-2}$ at low temperatures due to a increase of the relative dielectric permittivity $\epsilon_r = \chi + 1$ of STO [41].

REFERENCES

1. M.I. Dyakonov and V.I. Perel, *Chapter 2 - Theory of Optical Spin Orientation of Electrons and Nuclei in Semiconductors*, Modern Problems in Condensed Matter Sciences, edited by F.M.a.B.P. Zakarchenya, , Optical Orientation Vol. 8, pp. 11–71, Elsevier, 1984.
2. Y.K. Kato *et al.*, *Observation of the Spin Hall Effect in Semiconductors*, Science 306 (2004) 1910.

3. M.Z. Hasan and C.L. Kane, *Colloquium: Topological insulators*, Reviews of Modern Physics 82 (2010) 3045.
4. I. Žutić, J. Fabian and S. Das Sarma, *Spintronics: Fundamentals and applications*, Reviews of Modern Physics 76 (2004) 323.
5. M.N. Baibich *et al.*, *Giant Magnetoresistance of (001)Fe/(001)Cr Magnetic Superlattices*, Physical Review Letters 61 (1988) 2472.
6. G. Binasch *et al.*, *Enhanced magnetoresistance in layered magnetic structures with antiferromagnetic interlayer exchange*, Physical Review B 39 (1989) 4828.
7. J. Fabian *et al.*, *Semiconductor Spintronics*, Acta Physica Slovaca 57 (2007) 565.
8. N. Mott, Proceedings of the Royal Society of London A: Mathematical, Physical and Engineering Sciences Vol. 153, pp. 699–717, The Royal Society, 1936.
9. T. Valet and A. Fert, *Theory of the perpendicular magnetoresistance in magnetic multilayers*, Physical Review B 48 7099.
10. M. Johnson and R.H. Silsbee, *Calculation of nonlocal baseline resistance in a quasi-one-dimensional wire*, Physical Review B 76 (2007) 153107.
11. F.L. Bakker *et al.*, *Interplay of Peltier and Seebeck Effects in Nanoscale Nonlocal Spin Valves*, Physical Review Letters 105 (2010) 136601.
12. F. Volmer *et al.*, *Contact-induced charge contributions to non-local spin transport measurements in Co/MgO/graphene devices*, 2D Materials 2 (2015) 024001.
13. A.M. Kamerbeek, Charge and spin transport in Nb-doped $SrTiO_3$ using Co/AlO_x spin injection contacts, PhD thesis, University of Groningen, 2016.
14. F. Jedema, Electrical spin injection in metallic mesoscopic spin valves, PhD thesis, University of Groningen, 2002.
15. F.J. Jedema *et al.*, *Electrical detection of spin accumulation and spin precession at room temperature in metallic spin valves*, Applied Physics Letters 81 (2002) 5162.
16. M. Wojtaszek, I.J. Vera-Marun and B.J. van Wees, *Transition between one-dimensional and zero-dimensional spin transport studied by Hanle precession*, Phys. Rev. B 89 (2014) 245427.
17. S.P. Dash *et al.*, *Electrical creation of spin polarization in silicon at room temperature*, Nature 462 (2009) 491.
18. G. Schmidt *et al.*, *Fundamental obstacle for electrical spin injection from a ferromagnetic metal into a diffusive semiconductor*, Phys. Rev. B 62 (2000) R4790.
19. A. Fert and H. Jaffrès, *Conditions for efficient spin injection from a ferromagnetic metal into a semiconductor*, Physical Review B 64 (2001) 184420.
20. R.J. Elliott, *Theory of the Effect of Spin-Orbit Coupling on Magnetic Resonance in Some Semiconductors*, Physical Review 96 (1954) 266.
21. Y. Yafet, *g Factors and Spin-Lattice Relaxation of Conduction Electrons*, Solid State Physics, edited by F.S.a.D. Turnbull Vol. 14, pp. 1–98, Academic Press, 1963.
22. M.I. D'yakonov and V.I. Perel', *Spin Orientation of Electrons Associated with the Interband Absorption of Light in Semiconductors*, Journal of Experimental and Theoretical Physics 33 (1971) 1053.
23. E.Y. Tsymbal and I. Zutic, Handbook of Spin Transport and Magnetism (CRC Press, 2016).
24. Y.A. Bychkov and E.I. Rashba, *Oscillatory effects and the magnetic susceptibility of carriers in inversion layers*, Journal of Physics C: Solid State Physics 17 (1984) 6039.
25. Y.A. Bychkov and E.I. Rashba, *Properties of a 2D electron gas with lifted spectral degeneracy*, JETP Letters 39 (1984) 78.
26. A. Manchon *et al.*, *New perspectives for Rashba spin-orbit coupling*, Nature Materials 14 (2015) 871.
27. K.S. Novoselov *et al.*, *Electric Field Effect in Atomically Thin Carbon Films*, Science 306 (2004) 666.
28. P.R. Wallace, *The Band Theory of Graphite*, Physical Review 71 (1947) 622.
29. T.B. Coplen *et al.*, *Isotope-abundance variations of selected elements (IUPAC Technical Report)*, Pure and Applied Chemistry 74 (2002).
30. W. Han *et al.*, *Graphene spintronics*, Nature Nanotechnology 9 (2014) 794.

31. N. Tombros *et al.*, *Electronic spin transport and spin precession in single graphene layers at room temperature*, Nature 448 (2007) 571.
32. P.J. Zomer *et al.*, *Long-distance spin transport in high-mobility graphene on hexagonal boron nitride*, Physical Review B 86 (2012) 161416.
33. W. Han *et al.*, *Tunneling Spin Injection into Single Layer Graphene*, Phys. Rev. Lett. 105 (2010) 167202.
34. M. Guimarães *et al.*, *Controlling Spin Relaxation in Hexagonal BN-Encapsulated Graphene with a Transverse Electric Field*, Physical Review Letters 113 (2014) 086602.
35. K.F. Mak *et al.*, *Atomically Thin MoS_2: A New Direct-Gap Semiconductor*, Physical Review Letters 105 (2010) 136805.
36. K.v. Benthem, C. Elsässer and R.H. French, *Bulk electronic structure of SrTiO3: Experiment and theory*, Journal of Applied Physics 90 (2001) 6156.
37. K.A. Müller and H. Burkard, *$SrTiO_3$: An intrinsic quantum paraelectric below 4 K*, Physical Review B 19 (1979) 3593.
38. J.A. Sulpizio *et al.*, *Nanoscale Phenomena in Oxide Heterostructures*, Annual Review of Materials Research 44 (2014) 117.
39. A.M. Kamerbeek, T. Banerjee and R.J.E. Hueting, *Electrostatic analysis of n-doped $SrTiO_3$ metal-insulator-semiconductor systems*, Journal of Applied Physics 118 (2015) 225704.
40. K.G. Rana, V. Khikhlovskyi and T. Banerjee, *Electrical transport across Au/Nb:$SrTiO_3$ Schottky interface with different Nb doping*, Applied Physics Letters 100 (2012) 213502.
41. A. Spinelli *et al.*, *Electronic transport in doped $SrTiO_3$: Conduction mechanisms and potential applications*, Physical Review B 81 (2010) 155110.